# Mineralogical investigations using XRD, XRF and Raman Spectroscopy in a combined approach

**Maria Secchi[1], Marco Zanatta[2], Evgeny Borovin[1], Mauro Bortolotti[1], Arun Kumar[2], Marco Giarola[2], Andrea Sanson[3], Beate Orberger[4,5], Nicola Daldosso[2], Stefano Gialanella[1], Gino Mariotto[2], Maurizio Montagna[6], Luca Lutterotti[1]**

[1] *University of Trento, Department of Industrial Engineering, via Sommarive 9, 38123 Trento, maria.secchi@unitn.it*
[2] *University of Verona, Department of Computer Science, Ca' Vignal 2, Strada le Grazie 15, 37134 Verona*
[3] *University of Padua, Department of Physics, via Marzolo 8, 35131 Padova*
[4] *ERAMET-RESEARCH-SLN, 1 Avenue Albert Einstein, 78190 Trappes, France*
[5] *GEOPS, Université Paris Sud, Bât 504, 91405 Orsay Cedex, France*
[6] *University of Trento, Department of Physics, via Sommarive 14, 38123 Trento*

## Abstract

The identification of mineralogical phases in drill cores is one of the most challenging tasks in the mining activity in view of an efficient metal extraction. This process requires the analytical characterization of large volumes of material to obtain a complete set of data in a minimum of time. None of the commonly used methods in mineralogical analyses, such as IR based techniques, X-rays fluorescence, and hyperspectral imagining, is capable to provide a fully satisfactory response for several reasons, the main one being the complexity of the ores. Moreover, the characterization is often conducted in remote laboratories and only on selected samples to limit the time waste. A possible alternative solution requires a multi-analytical approach exploiting on-field techniques. This strategy is currently being developed within SOLSA, a joint EU H2020 project, and consists of an automatic expert system coupling sonic drilling, imaging, profilometer, hyperspectral cameras, and a combination of Raman spectroscopy, X-rays fluorescence, and X-rays diffraction. In this work, the principles on which this cooperative approach is based are discussed, with application to two specific test samples, showing the potential and novelty of the method. In particular, a case is considered in which the sample characterization by the separate use of a single technique fails, whereas the combination of the three analyses (Raman spectroscopy, X-rays fluorescence, X-rays diffraction) works even if the system is very complex.

**Keywords**: combined analysis, mineralogical phase identification, Raman, XRF, XRD

## INTRODUCTION

Quantitative mineralogical and chemical analyses of ores are paramount for an efficient survey and subsequent mining and extraction processes. Another key aspect, considering the large volumes of the samples to be investigated, is the possibility to get a full set of data in a comparatively short time and by using on-field instrumentation in order to not move around large samples (e.g., core drills). Nowadays, the typical analyses performed on mine drill cores for the identification of mineralogical phases are carried out by preparing the samples in thin sections, which are then separately analysed by means of different techniques, like electron micro-probe analysis (EPMA) and scanning electron microscopy (SEM)[1,2]. X-rays based techniques such as X-ray diffraction (XRD) and X-ray fluorescence (XRF) are widely used in the geological field for the non-destructive characterization of unknown samples. In particular, XRD is adopted to determine and to quantify the mineralogical phases, for microstructure and texture analysis and *ab initio* structure determination. Conversely, XRF is used for quantitative chemical characterization of materials. However, both these techniques present also several limitations for the characterization of geological samples: in fact, the detection limit of XRD of low phase content is at least 1% in weight in the typical laboratory condition, i.e. no minor phases can be detected. Moreover, the presence of amorphous components cannot be accurately determined by XRD, while organic materials are not easily handled by both XRD and XRF. XRF analysis, carried out in environmental conditions, can in general detect chemical elements with atomic number higher than that of silicon, and the minimum measurable concentration ranges from 10 ppm for heavy elements up to several weight percents for light elements.

On the other hand, Raman spectroscopy (RS) is also a widely used technique in the geological field for its capability to detect organic, inorganic, crystalline and amorphous materials, and for the possibility to be used in a micro-sampling configuration either in the laboratory instruments or in portable systems. RS can be regarded as a substantially non-destructive technique, a plus for some specific applications, in particular for on-field investigations. The determination of the mineralogical phases with RS is usually performed by comparing the experimental data with reference standards. However, RS provides only a qualitative information on the presence of mineralogical phases being in general not possible to quantify their abundance, except on statistical basis using a very fine sampling of the material[3].
It has already been demonstrated[4,5] that the combined application of XRD and XRF from both an experimental and analytical point of view is a powerful tool for material characterization. The extension of the combined approach also to RS for the phase identification and quantification in drill core samples is part of the objectives of the SOLSA project (G.A. No. 689868), funded by the EU-H2020 Raw materials framework. The main target of SOLSA is the design and the realization of an expert system coupling sonic drilling machine and a multi-technique characterization instrument suitable for on-line real-time on-site analyses of drill cores from geological and mining surveys[6]. At present, a non-negligible part of the costs of a mining project are for exploration and processing. Indeed, exploration is based on data obtained from the chemical and mineralogical analyses of drill core samples performed in laboratories far from the mine sites, thus taking comparatively long times. The reliability of the data, the representativeness of the samples and the short acquisition time are crucial aspects for a test procedure developed to estimate the potential yield of a mining site. Mineralogical and chemical data are needed for optimizing the mining process. At present, these data are mostly obtained by using a single technique, like XRF scanner or hyperspectral imaging[7–9]. A combined, multi-technique analytical characterization of drill cores can be the solution for speeding up exploration and mining, thus reducing mining costs and environmental impact. However, the combination of different characterization technique to obtain accurate and reliable results on drill cores is still a technological challenge. The multi-technique instrument, which is under development within the SOLSA project, is based on coupling of hyperspectral imaging, XRF, XRD, and RS.

In this work, two different lithologies, a siliceous breccia and a serpentinized harzburgite, have been characterized by means of XRF, XRD and RS with the aim of presenting and discussing the principles on which the cooperative approach is based, and of showing advantages as well as challenges for the involved techniques. Scanning electron microscopy (SEM) and Energy Dispersive X-rays Spectroscopy (EDXS) have been used to confirm the results obtained by the other three characterization methods.

## EXPERIMENTAL

### Materials

The experimental work has been focused on the characterization of two samples, representative of the typical materials available within the SOLSA project: (a) siliceous breccia (SB), a rock originated from hydrofracturing of ultramafic rocks, mainly composed of quartz, and (b) serpentinized harzburgite, dark green peridotite (HN0), coarsed to medium grained, mainly composed by orthopyroxene, olivine, and serpentine. Both the analysed samples were in form of discs diamond-cut out from core drills (Fig.1).

a) b)

*Fig. 1. Samples characterized within this work are discs cut from core drills. (a) Siliceous breccia (SB), and (b) dark green peridotite (HN0). Their diameters are 63.5 mm.*

These samples have been selected since they can be considered as end-members in terms of complexity of the mining materials relevant for the SOLSA project. In fact, the first one (SB) is a simple material characterized by the presence of a small number of mineralogical phases, the second (HN0) is complex system characterized by the presence of veins and grains constituted by several different phases.

**Methods**

Micro-Raman spectroscopy (μRS) measurements were carried out with two instruments, a Horiba Labram HR (spectrograph focal length: 800 mm; excitation wavelength: 633 nm He-Ne laser) and a Horiba Labram Aramis (spectrograph focal length: 450 mm; excitation wavelength: 785 nm IR-laser diode). Both instruments are equipped with a 600 lines/mm grating and the experimental resolutions are 1.5 and 3 $cm^{-1}$, respectively. Micro-sized regions with a diameter of about 3 μm and 5 μm were probed using two long working distance (LWD) objectives, an 80x and a 50x, respectively. The laser powers at the sample are 6 mW and 25 mW, respectively. However, in order to avoid laser-induced heating and consequent modifications of the mineral phases [e.g. [10]], the effects of the laser power at the sample were carefully monitored and adjusted by means of appropriate neutral filters whose optical density was between 0.3 and 1.

X-ray diffraction measurements were performed on a Rigaku DMAX III diffractometer working in Bragg-Brentano geometry, equipped with a 2 kW Cu source on the primary beam and a scintillation counter coupled to a graphite monochromator on the secondary beam. The use of a diffracted beam monochromator was required to suppress the induced sample fluorescence due to iron presence. A 3-120 deg 2θ range was acquired, with 0.02 deg steps and 10 second counting time, providing excellent resolution and signal statistics. X-ray fluorescence spectra were acquired using an Inel Equinox 3500 combined XRD/XRF spectrometer, equipped with a Mo microfocus source and parabolic multilayer mirror on the primary beam and an Amptek X-123SDD Silicon Drift Detector placed vertically 10 mm over the sample to ensure high sensitivity even with low-atomic number elements; XRF data was collected for 600 seconds for each sample. For both X-rays techniques, the irradiated sample area is about 8×4 $mm^2$ and 6×0.2 $mm^2$, respectively. The penetration depth varies from a few microns to several tens of microns for the Cu and Mo sources, respectively. The so-obtained results can be thus interpreted as an average signal of chemical and crystallographic composition of the samples.

A suitable sequence for the combined analysis consists of XRF, followed by μRS and then by XRD, possibly using also XRF data. However, key elements for such an approach are proper reference databases for the identification of XRD and μRS data.

As first step, XRF can be used as a stand-alone probe, providing the identification of elements heavier than magnesium through a full-pattern fit using the Maud program[11]. This input allows a first selection among possible phases included in the databases. The identification of mineralogical phases using μRS is obtained by comparing experimental spectra, after a careful subtraction of the luminescence background, with reference spectra present in the RRUFF database using the software CrystalSleuth[12]. Indeed, a single Raman spectrum could not represent the whole mineralogical composition of the sample. However, μRS spectra are often characterized by only a few phases, or by a single phase if the crystalline grains have a volume larger than that of excitation, thus easing their identification. This qualitative assessment of phases provides a further starting guess for XRD analysis. This allows to select a subset of the Crystallography Open Database[13], by filtering the entries non containing the chemical elements found by XRF, and adding or confirming the phases found by RS. The phases present in the diffraction pattern are identified via an iterative search-match procedure[14]. Every candidate phase is compared against the experimental pattern and a score based on a full-profile fit figure-of-merit is assigned[15].

Starting from this qualitative crystallographic identification, a multi–phase mixture model is defined with the Maud program[11], serving as the basis for both the quantitative analysis of XRD and XRF. A simultaneous fitting of both the XRD and XRF data is performed, starting from the common structural description of the sample, by means of a radiation-matter interaction model taking into account both

elastic scattering and photoelectron absorption/fluorescence[4]. The XRD data are modelled by means of the classical Rietveld methodology[16], taking into account structural and microstructural parameters of the sample, as well as the instrumental characteristics (see Supporting Information). On the other hand, the elemental composition as well as the matrix effects are calculated directly from the crystallographic model and then used to model the XRF spectra by means of a fundamental parameters approach. The simulated XRD and XRF datasets are then fitted against their experimental counterpart, by optimizing the relevant parameters through a least-squares algorithm which minimizes the combined fitness function of the XRD and XRF residuals. Finally, the full pattern fit of both XRF and XRD provides a quantitative estimation of the volume fraction of each component.

Lastly, to cross-check the results obtained by the above described methods, SEM and Energy Dispersive X-rays Spectroscopy (EDXS) observations were performed with a JEOL JSM-IT300LV microscope at high vacuum, by setting 20 kV tension. Samples were polished, dried and coated with Pt-Pd alloy. The elemental surface distribution was analysed by the means of EDXS mapping.

## RESULTS

### Case study 1: Siliceous breccia

The XRF analysis shows the presence of silicon, iron and other metals in traces (Table 1 and Fig. 2(a)). XRD data analysis reveals that the sample is 100% composed by quartz with an extremely good fitting (Fig.2(b)). In particular, no iron or other metal oxides, hydroxides or more complex minerals have been found, conversely to what observed with XRF.

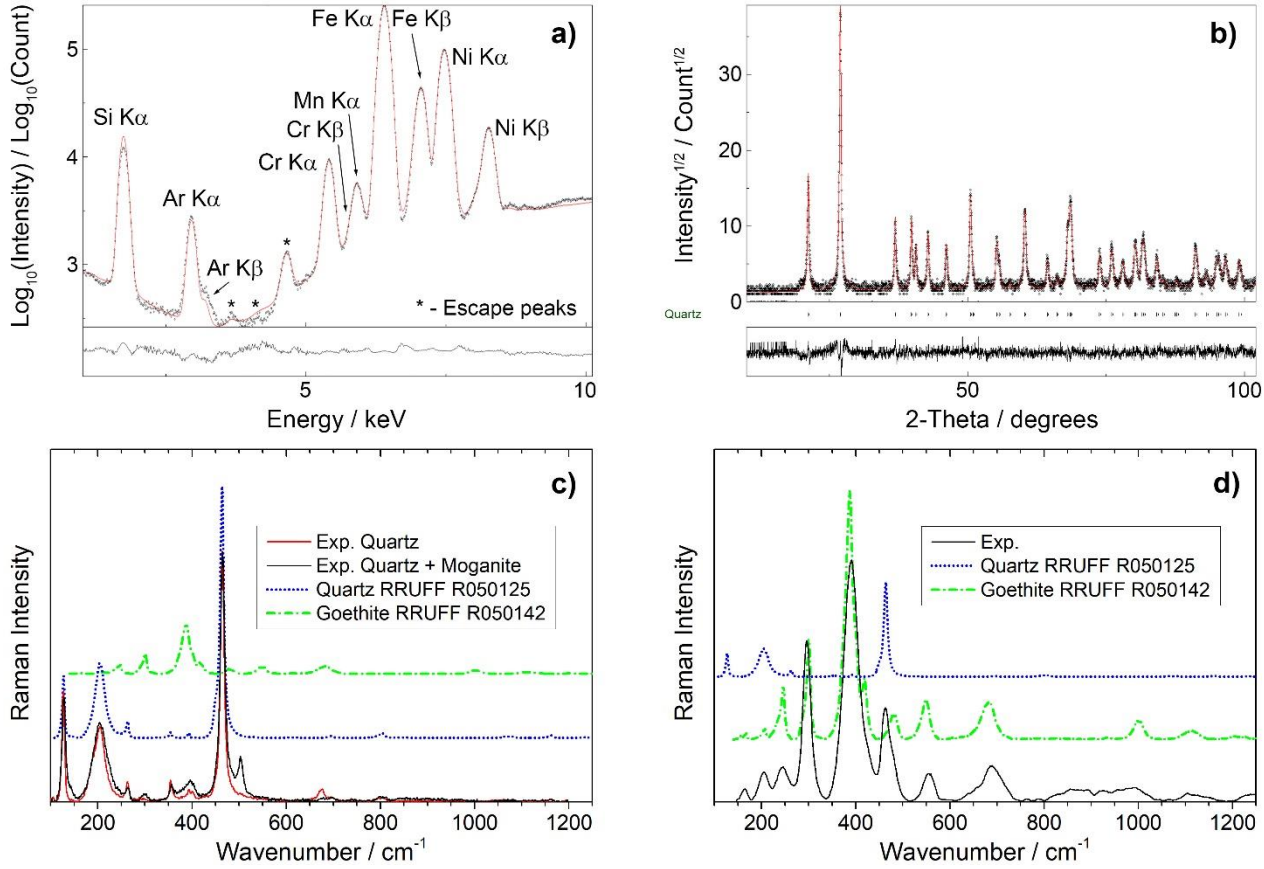


*Fig. 2. Siliceous breccia (SB): (a) XRF spectrum, the most important lines are indicated. (b) XRD pattern, where the black dots are the experimental data, the red line is the fit, and the black line in the bottom box is the difference between the data and the fit function. XRD pattern represents solely quartz phase (α-$SiO_2$). (c) – (d) Raman spectra collected on two different sample micro-regions, and compared with reference spectra of RRUFF database. In (c)*

*the spectra are collected by using the 785 nm laser line, in (d) the 633 nm laser line. The presence of quartz, moganite, and goethite is shown.*

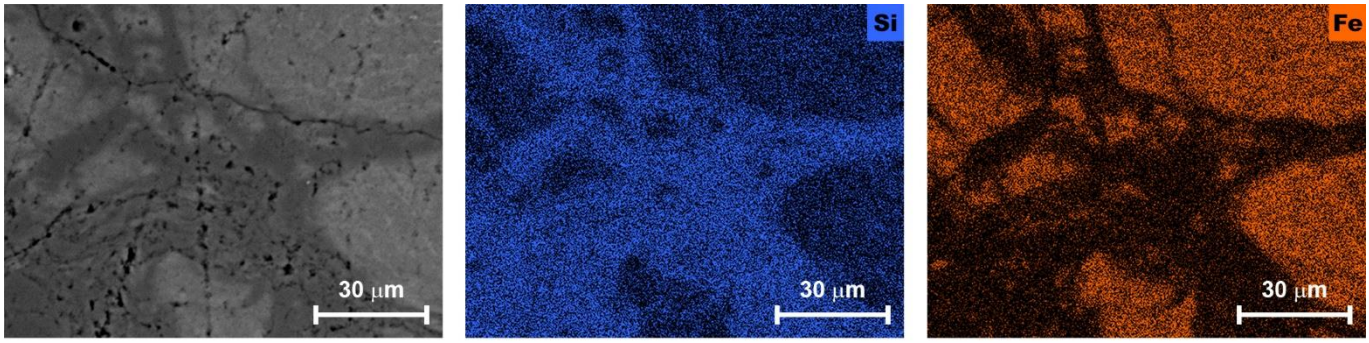


*Fig. 3. Siliceous breccia (SB): (a) SEM image, (b) – (c) EDXS elemental content. (b) Silicon and (c) iron are detected.*

An extensive investigation of the sample surface by μRS shows that Sample SB appears mainly constituted by quartz (α-$SiO_2$) with some inclusions of hematite (α-$Fe_2O_3$) and goethite (FeO(OH)), characterized by the typical red color. The high spatial resolution of μRS allows to select different grains obtaining spectra where the contribution of a single phase is dominant. In most spectra quartz is observed as the dominant phase. At several investigation points, the presence of moganite, a polymorph of quartz, is also detected (Fig. 2(c)). Its peculiar Raman fingerprint occurs at about 500 $cm^{-1}$, whereas quartz main peak is at about 460 $cm^{-1}$[17]. Therefore, the presence of this polymorph is evident according to the RS data. This phase was not detected by XRD.

However, spectra of a single phase are rarely detected. Both Raman spectra of Fig. 2 show the co-existence of two or more phases. In Fig. 2(c) the dominant contribution is from quartz with a minor contribution of moganite, and a weak contribution of goethite. On the other hand, Fig. 2(d) shows a spectrum taken in a 'red' region, where the contribution of goethite is dominant. The comparison of results of the Figs. 2(c) and 2(d) draws the attention to an important problem related to the use of Raman databases. The spectrum of Fig. 2(c) has been obtained by excitation by the 785 nm laser line with a resolution comparable to those of the RRUFF references, and nevertheless the quartz, moganite, and goethite spectral definition differs. In contrast, the spectrum of Fig. 2(d), obtained by excitation by the 633 nm laser line has a lower resolution. This makes a quantitative analysis by an automatic software more difficult.

The iron detected by XRF can be ascribed, according to Raman measurements, to iron oxides inclusions, that have not been detected by XRD, since probably present in concentration below the detection limit of about 3 wt.%. In fact, the 3.1 wt.% of iron measured by XRF (Table 1) gives an upper limit of the goethite presence (5 wt.%), assuming that all the iron is related to this phase. However, Raman spectra showed the presence of both hematite and goethite, and furthermore, as it will be discussed in the next paragraph, EDXS analysis shows that Fe is present also in the quartz matrix, likely as micro- or nano-inclusions.

SEM and EDXS analyses confirm the dominant presence of Si with inclusions constituted by Si-free and Fe-rich phases. Figure 3 shows EDXS elemental mapping data in a region where a Si-rich phase and a Fe-rich phase have comparable importance. Therefore, the results obtained by combining XRF and XRD data with a multiple sampling with μRS are verified. Other trace elements detected by XRF, such as Ni, Co, and Mn, are probably substituting the Fe sites of goethite, accordingly to Goldschmidt substitutional rules[18].

**Case study 2: Serpentinized harzburgite (HN0)**

XRF detects the presence of Mg, Si, Ca, Cr, Fe and Ni (spectrum not shown). The fitting of XRD pattern is non-trivial due to the high number of low-symmetry composing phases and their complex microstructure (Fig. 4). RS results were in this case fundamental to select the phases for the fitting of XRD. The diffraction pattern shows typical effect of turbostratic disorder as strongly asymmetric broad

shape of some peaks[19], whereas some other extremely narrow peaks suggest the presence of highly crystalline phases. Lizardite ($Mg_3(Si_2O_5)(OH)_4$) mineral was identified in the sample as main constituent, with various microstructure features. In order to model the studied sample three lizardite crystal structures were used with various crystallite sizes, cell parameters and disorders in microstructure. In particular, the turbostratic disorder was taken into account by introducing the Ufer correction [20].

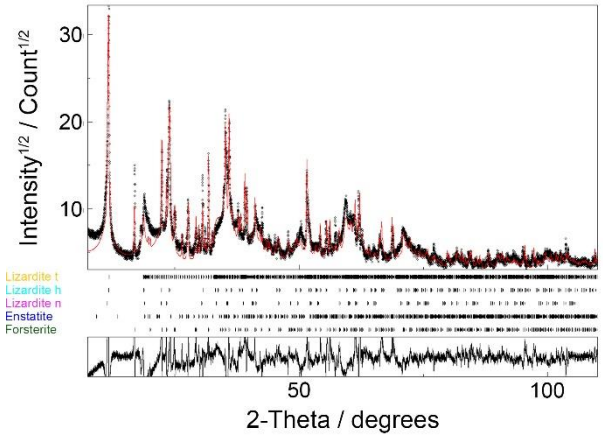


*Fig. 4. Serpentinized harzburgite (HN0): XRD pattern, where the black dots are the experimental data, the red line is the fit, and the black line in the bottom box is the difference between the data and the fit function. XRD pattern shows three microstructurally different lizardite phases: t – turbostratically disordered, h – highly crystalline and n - nano- crystalline phase.*

Coherently with this picture, also all acquired Raman spectra turn out to be rather complex. In fact, almost every Raman spectrum shows the presence of two or more phases (Fig. 5(a)). Differently from the previous case (sample SB), in HN0 the dominant phase is difficult to be determined by µRS, since more than 10 different mineralogical phases are observed. The most common ones are forsterite ($Mg_2(SiO_4)$), lizardite ($Mg_3(Si_2O_5)(OH)_4$), and some inclusions of goethite (FeO(OH)) (Fig. 5(a)-(b)). Also small amount of enstatite ($MgSiO_3$), magnesiochromite ($Mg(Cr, Al, Fe)_2O_4$), talc ($H_2Mg_3(SiO_3)_4$), quartz ($SiO_2$), cowlesite (zeolite) ($Ca(Al_2Si_3O_{10}(H_2O)$), and dwornikite (Ni, Fe)($SiO_4$)($H_2O$)) have been detected (not shown).

The unambiguously discrimination of lizardite from other polymorphs of the serpentine group, as chrysotile, antigorite, and polygonal serpentine, all having quite similar Raman spectra, was possible by observing the band shape in the spectral region of the OH stretching at about 3700 $cm^{-1}$. The Raman spectra of these minerals have been deeply studied[21–24], showing that the low wavenumber vibrational modes are very close and can be easily confused, even with the present resolutions. Conversely, the most important difference in the spectra is the shape of the OH stretching band, observable in a more extended spectrum that covers also this high wavenumber region (inset of Fig. 5(b))[21]. In fact, the vibrations of the OH groups allow to investigate the local geometry at the atomic scale, since they are sensitive to variations in the arrangement of the crystalline layers; moreover, the number and position of the OH stretching bands are influenced by the cell size and the symmetry of the crystal. Consequently, each polymorph presents a characteristic spectrum, related to its local structure. In particular, the peak shown in the inset of Fig. 5(b) is characterized by an intense peak at 3685 and an appreciable shoulder at 3700 $cm^{-1}$. These are fingerprints of lizardite, as reported in Ref. [21].

The presence of several phases in one single spectrum and the possible presence of polymorphic compounds makes the automatization of the phase identification a non-trivial task.

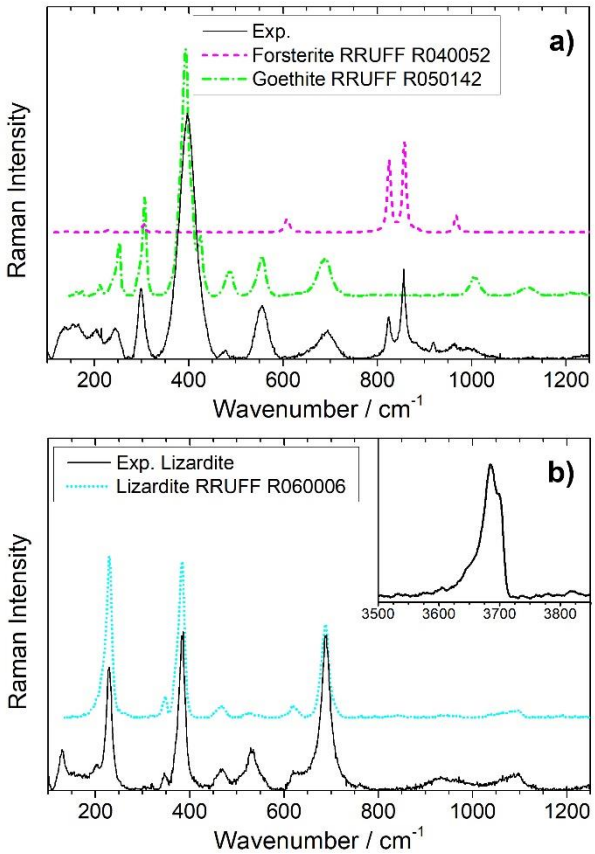


*Fig. 5. Serpentinized harzburgite (HN0): (a) – (b) Raman spectra collected on two different points of the sample (laser line: 633 nm), and compared with RRUFF references. Raman measurements show the presence of forsterite, goethite, and lizardite.*

This sample is the typical case in which the information from μRS, XRF, and XRD are all fundamental to achieve a reliable phase identification. In fact, Raman results have been used to reduce the XRD database for fitting by suggesting the phases to be imposed. The combination of these techniques indicates the presence of lizardite (76.5%), forsterite (15.8%), and enstatite (7.7%). As expected, XRD does not detect all the phases found by Raman measurements, when their concentration is below the detection limit.

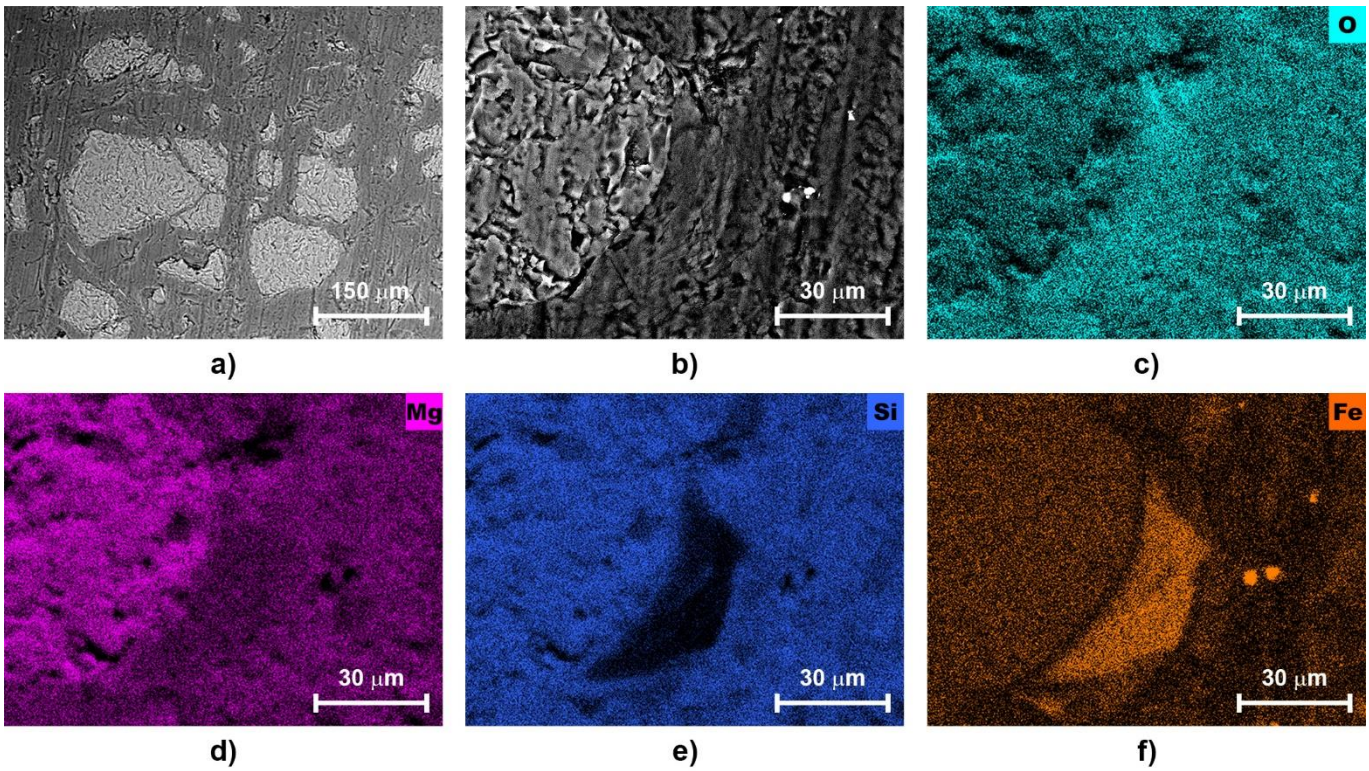


*Fig. 6. Serpentinized harzburgite (HN0): (a)-(b) SEM images at different magnifications, (c) – (f) EDXS elemental content related to image b area. (c) O, (d) Mg, (e) Si, and (f) Fe are detected.*

SEM images show the typical microstructure of the serpentinized harzburgite (Figs. 6(a)-(b)). EDXS analysis confirms the presence of a Mg-Si-O-rich phase, probably a magnesium silicate (Fig. 6(c)-(e)). Moreover, Fe-rich inclusions are detected (Fig. 6(f), bright contrast). However, it is worth noting that iron is also present in the magnesium silicate region, suggesting Fe as a substitutional ion at Mg sites.
Further SEM-BSE and EDXS analyses performed on the second sample (Fig. S1 in the Supporting Information) confirm its complexity, as expected for a natural mineralogical sample.

## CONCLUSIONS

In this work we showed the potentialities of a combined approach exploiting μRS, XRF, and XRD to identify the mineral phases in geological samples. The quantitative determination of the phase composition can be obtained by a combined full-pattern Rietveld analysis of XRD and XRF data. However, the bottleneck of such an approach is the identification of the phases. For materials with simple mineralogy the search-match approach gives unambiguous results. Conversely, for heterogeneous systems further inputs are necessary and these can be provided by micro-Raman spectroscopy. Indeed, while XRD and XRF probe macroscopic areas (on the order of a few square millimetres), micro-Raman operates on a few microns. This implies that, even for complex systems, Raman spectra typically contain a few phases, ideally one, thus easing their identification. The qualitative input from μRS effectively constrains the search-match algorithm.
This is clearly shown by the two case studies. The first, siliceous breccia, has a simple mineralogy and the combination of XRD and XRF gives a quantitative assessment of the mineral phases. Raman spectroscopy confirms the same main mineralogy and adds information on very local inclusions that are beyond the XRD sensitivity. In fact, XRD shows only the presence of quartz but Raman spectroscopy detects also goethite and hematite, explaining the presence of the iron-rich phases observed by XRF and confirmed by SEM. On the other hand, harzburgite is a typical example of a complex material for which the separate use of a single experimental technique fails in providing a reliable characterization. Only the combination of XRF, XRD and Raman within the outlined approach allowed a quantitative result even on this system.

This analytical approach will be implemented on a dedicated expert system within the SOLSA project. This multi-technique instrument will be optimized to provide a reliable tool for real-time analysis directly on-mine. In this apparatus, Raman measurement can be acquired by automatically mapping the same surface probed by XRF and XRD. The only limit to the statistical representativeness of such a mapping is the acquisition time that needs to be balanced among the different techniques. However, Raman spectroscopy is confirmed to be a powerful technique for geological samples that can substitute analytical techniques, like SEM, in particular when portability issues become crucial.

**Acknowledgements**
The authors thank all the SOLSA partners for the collaboration, in particular: F. Trotet, M. Kadar and K. Devaux (ERAMET-SLN, New Caledonia), A. Salaün and C. Rodriguez (ERAMET) for providing the samples, M. Le Guen (ERAMET) for useful discussions. This work has been developed within the SOLSA project (www.solsa-mining.eu) founded by the European Commission through H2020 programme (SC5-11d-689868).

**References**

[1] S. Sindern, F.M. Meyer, *Phys. Sci. Rev.* **2016**; 1, 9.
[2] P. Gottlieb, G. Wilkie, D. Sutherland, E. Ho-Tun, S. Suthers, K. Perera, B. Jenkins, S. Spencer, A. Butcher, J. Rayner, *JOM* **2000**; 52, 4.
[3] D.R. Neuville, D. De Ligny, G.S. Henderson, *Rev. Mineral. Geochemistry* **2014**; 78.
[4] M. Bortolotti, L. Lutterotti, G. Pepponi, *Powder Diffr.* **2017**; 32, S1.
[5] L. Lutterotti, F. Dell'Amore, D.E. Angelucci, F. Carrer, S. Gialanella, *Microchem. J.* **2016**; 126.
[6] http://www.solsa-mining.eu, .
[7] T.J. Cudahy, R.D. Hewson, M.S. Caccetta, A. Roache, L.B. Whitbourn, P. Connor, D.A. Coward, P. Mason, K. Yang, J.F. Huntington, M. Quigley, *Rev. Econ. Geol.* **2009**; 16.
[8] T.J. Roache, J.L. Walshe, J.F. Huntington, M.A. Quigley, K. Yang, B.W. Bil, K.L. Blake, T. Hyvärinen, *Aust. J. Earth Sci.* **2011**; 58, 7.
[9] M. Haest, T. Cudahy, C. Laukamp, S. Gregory, *Econ. Geol.* **2012**; 107, 2.
[10] S. Gialanella, F. Girardi, G. Ischia, I. Lonardelli, M. Mattarelli, M. Montagna, *J. Therm. Anal. Calorim.* **2010**; 102, 3.
[11] L. Lutterotti, M. Bortolotti, G. Ischia, I. Lonardelli, H.-R. Wenk, *Zeitschrift Fur Krist. Suppl.* **2007**; 1, 26.
[12] B. Lafuente, R.T. Downs, H. Yang, N. Stone, 1. The power of databases: The RRUFF project, in: Highlights Mineral. Crystallogr., DE GRUYTER, Berlin, München, Boston, **2016**; pp. 1–30.
[13] S. Gražulis, A. Daškevič, A. Merkys, D. Chateigner, L. Lutterotti, M. Quirós, N.R. Serebryanaya, P. Moeck, R.T. Downs, A. Le Bail, *Nucleic Acids Res.* **2012**; 40, D1.
[14] L. Lutterotti, http://cod.iutcaen.unicaen.fr/.
[15] L. Lutterotti, H. Pilliere, C. Fontugne, P. Boullay, D. Chateigner, http://cod.iutcaen.unicaen.fr/.
[16] H.M. Rietveld, *J. Appl. Crystallogr.* **1969**; 2, 2.
[17] P. Schmidt, L. Bellot-Gurlet, V. Leá, P. Sciau, *Eur. J. Mineral.* **2013**; 25, 5.
[18] V.M. Goldschmidt, *J. Chem. Soc.* **1937**; 0.
[19] L. Lutterotti, M. Voltolini, H.-R. Wenk, K. Bandyopadhyay, T. Vanorio, *Am. Mineral.* **2010**; 95, 1.
[20] K. Ufer, G. Roth, R. Kleeberg, H. Stanjek, R. Dohrmann, J. Bergmann, *Zeitschrift Für Krist. - Cryst. Mater.* **2004**; 219, 9.
[21] J.R. Petriglieri, E. Salvioli-Mariani, L. Mantovani, M. Tribaudino, P.P. Lottici, C. Laporte-Magoni, D. Bersani, *J. Raman Spectrosc.* **2015**; 46, 10.
[22] C. Groppo, C. Rinaudo, S. Cairo, D. Gastaldi, R. Compagnoni, *Eur. J. Mineral.* **2006**; 18, 3.
[23] A.-L. Auzende, I. Daniel, B. Reynard, C. Lemaire, F. Guyot, *Phys. Chem. Miner.* **2004**; 31, 5.
[24] M. Cathelineau, A. Myagkiy, B. Quesnel, M.-C. Boiron, P. Gautier, P. Boulvais, M. Ulrich, L. Truche, F. Golfier, M. Drouillet, *Miner. Depos.* **2017**; 52, 7.

| Element | Wt.% | At.% |
|---|---|---|
| Si | 43.9 | 32.3 |
| O | 51.8 | 66.5 |
| Fe | 3.1 | 0.9 |
| Ni | 0.7 | 0.2 |
| Cr | 0.2 | 0.06 |
| Mn | 0.05 | 0.01 |
| Co | 0.02 | 0.005 |

*Table I. Elemental composition of sample SB in weight and in atomic percentage, as obtained from XRF measures.*